Nanoscale

PAPER

View Article Online
View Journal | View Issue

Cite this: *Nanoscale*, 2018, **10**, 12743

Probing the influence of cell surface polysaccharides on nanodendrimer binding to Gram-negative and Gram-positive bacteria using single-nanoparticle force spectroscopy

Audrey Beaussart, *[a] Christophe Beloin, [b] Jean-Marc Ghigo,[b] Marie-Pierre Chapot-Chartier, [c] Saulius Kulakauskas [c] and Jérôme F. L. Duval [a]

The safe use and design of nanoparticles (NPs) ask for a comprehensive interpretation of their potentially adverse effects on (micro)organisms. In this respect, the prior assessment of the interactions experienced by NPs in the vicinity of – and in contact with – complex biological surfaces is mandatory. It requires the development of suitable techniques for deciphering the processes that govern nano-bio interactions when a single organism is exposed to an extremely low dose of NPs. Here, we used atomic force spectroscopy (AFM)-based force measurements to investigate at the nanoscale the interactions between carboxylate-terminated polyamidoamine (PAMAM) nanodendrimers (radius *ca.* 4.5 nm) and two bacteria with very distinct surface properties, *Escherichia coli* and *Lactococcus lactis*. The zwitterionic nanodendrimers exhibit a negative peripheral surface charge and/or a positive intraparticulate core depending on the solution pH and salt concentration. Following an original strategy according to which a single dendrimer NP is grafted at the very apex of the AFM tip, the density and localization of NP binding sites are probed at the surface of *E. coli* and *L. lactis* mutants expressing different cell surface structures (presence/absence of the O-antigen of the lipopolysaccharides (LPS) or of a polysaccharide pellicle). In line with electrokinetic analysis, AFM force measurements evidence that adhesion of NPs onto pellicle-decorated *L. lactis* is governed by their underlying electrostatic interactions as controlled by the pH-dependent charge of the peripheral and internal NP components, and the negatively-charged cell surface. In contrast, the presence of the O-antigen on *E. coli* systematically suppresses the adhesion of nanodendrimers onto cells, may the apparent NP surface charge be determined by the peripheral carboxylate groups or by the internal amine functions. Altogether, this work highlights the differentiated roles played by surface polysaccharides in mediating NP attachment to Gram-positive and Gram-negative bacteria. It further demonstrates that the assessment of NP bioadhesion features requires a critical analysis of the electrostatic contributions stemming from the various structures composing the stratified cell envelope, and those originating from the bulk and surface NP components. The joint use of electrokinetics and AFM provides a valuable option for rapidly addressing the binding propensity of NPs to microorganisms, as urgently needed in NP risk assessments.

Received 29th March 2018,
Accepted 5th June 2018

DOI: 10.1039/c8nr01766b

rsc.li/nanoscale

Introduction

Engineered soft nanoparticles (NPs) have rapidly emerged in pharmaceutical and biomedical applications due to the versatility of options they offer in terms of chemical and physical functionalities.[1] Rationalizing NP design is essential to meet the best compromise between the performance for a given targeted purpose (*e.g.* diagnosis, drug delivery) and reduction of the bioadverse outcomes they may generate for humans and/or (micro)organisms once released in the environment at the end of their life cycle.[2] Providing a clear connection between the NP structure/composition and their toxicity is not a trivial task due to the complexity of the mechanisms that take place at bio-nano interfaces.[3] In order to address such a connection at a mechanistic level, it is essential to first evaluate the type and magnitude of the interaction forces operational between NPs and cell envelopes, the latter being known to confer/maintain cell shape, regulate internal turgor pressure or mediate (bio)

[a]*Université de Lorraine, CNRS, LIEC, F-54000 Nancy, France. E-mail: audrey.beaussart@univ-lorraine.fr*
[b]*Institut Pasteur, Unité Génétique des Biofilms, F-75724 Paris 15, France*
[c]*Micalis Institute, INRA, AgroParisTech, Université Paris-Saclay, 78350 Jouy-en-Josas, France*

adhesion. These interactions are determined by the physico-chemical surface/bulk properties of the NPs, the nature and density of biomolecules distributed over the cell surface (*e.g.* proteins and polysaccharides) and by the medium conditions (*e.g.* pH, salinity and temperature) that impact on the NP–cell surface encounter rate.

Representative examples of manufactured soft nanoparticles include (nano)dendrimers defined by an internal hyperbranched structure supporting amine charges and a peripheral layer whose composition can be tailored at will.[4,5] (Nano)dendrimers are now routinely employed in diverse technologies and fields such as catalysis, materials science and biology/medicine, where they serve *e.g.* as imaging agents, antimicrobial compounds or drug carriers.[6–10] While circulating in physiological media such as blood serum or in aquatic environments, NPs encounter a complex mixture of molecules (*e.g.* proteins, lipids and sugars) which may adsorb at their surface and modify their native physico-chemical properties.[11,12] All NPs then get decorated by a soft layer, a so-called 'protein corona'. Dendrimers are paradigms of soft nanoparticles (*i.e.* ion- and water-permeable) whose structure, size and composition can be easily modulated. As such, they are versatile, astonishingly stable (against aggregation, see our previous report)[13] and suitable model systems to mimic environmental NPs that often consist of a core component surrounded by a fuzzy (bio)macromolecular or proteinaceous corona.[14–16]

Despite the numerous functions dendrimers may offer,[17] their use is now debated following recent reports that evidence their potential cytotoxicity. In particular, they have been reported to favor cytotoxic and hemolytic actions due to the diversity of their targets, such as plasma membranes,[18] cell organelles (*e.g.* endosomes,[19] mitochondria,[20,21] and the nucleus)[22] and proteins such as enzymes.[23] The toxicity of full-generation cationic dendrimers has been mostly attributed to the interactions they experience with anionic cell membranes. The use of half-generation dendrimers carrying anionic peripheral groups was then suggested as an alternative to prevent attraction of such NPs to cells and therewith their subsequent ad/ab-sorptions on cell membranes.[2] In line with this reasoning, studies conducted *in vivo* with anionic dendritic NPs reported a toxicity that was less pronounced than that generated by their full generation counterparts.[24,25] However, as demonstrated in our recent work,[26] the sign of the effective charge of 'anionic' NPs with a negative surface charge and a positively charged inner core may change under slight modification of pH and/or concentration of a monovalent electrolyte in the dispersing medium.[13,26] In turn, a prediction of soft dendrimer toxicity towards (micro)organisms requires a full account not only of the physico-chemical NP surface features but also of those defining the NP bulk composition, both mediating – together with the biophysical properties of the membrane – the NP–cell interactions under aqueous conditions.

Well-studied and genetically amenable model bacteria represent suitable and controlled systems to address NP interactions with their envelopes. The distinct structures and compositions of Gram-negative and Gram-positive bacterial surfaces have been reported to interact differently with NPs.[27–31] In particular, Gram-negative bacterial LPS and Gram-positive bacterial teichoic acids are among the major biomolecules that possibly influence nanotoxicity as their presence/structure largely modulates bacteria–NP interactions.[32–37] Moreover, the use of genetic engineering allows an additional level of controlled investigation of bacterial–NP interactions *via* selective over-expression of genes encoding surface molecules or structures such as fimbriae, pili or LPS that inherently mediate the interactions of the whole cell with its surrounding environment.[38] Even though the initial interplay between NPs and surface polysaccharides is a recognized important step for adequate NP risk assessment, the evaluation of NP binding to cell envelopes at the relevant nanometric scale has received scant attention so far. This is mainly explained by a lack of appropriate techniques able to probe bio-physicochemical interactions involving NPs at the relevant single cell and single NP levels.

Atomic force microscopy and related single-molecule force spectroscopy have opened up new possibilities to assess bio-nano association interaction mechanisms with nanometer resolution and piconewton sensitivity.[39] Previous studies have reported the use of AFM-based force spectroscopy measurements to address dendrimer binding to abiotic surfaces decorated with proteins[40] or DNA.[41] However – to the best of our knowledge – dendrimer force spectroscopy on living bacteria has never been reported to date. In this work, by adopting an original strategy to decorate AFM tips with carboxylate-terminated polyamidoamine nanodendrimers (COOH-PAMAM), we demonstrate the performance of AFM-single NP force spectroscopy for addressing the differentiated adhesion of dendrimer NPs onto Gram-positive and Gram-negative bacteria, *L. lactis* and *E. coli*, respectively, genetically modified to express or not surface polysaccharides. Using independent electrophoretic mobility measurements performed on bacteria and NPs, we also show that NP binding to the cell surface is predominantly driven by electrostatic interactions, and that NP adhesion features are strongly mediated by both the polymeric biomolecules carried by the bacteria and the composition of the supporting cell wall structure.

Results and discussion

Bacterial cell surface imaging

The surface morphology of the bacteria of interest in this work was first imaged in a 10 mM KNO_3 background electrolyte using AFM (Fig. 1). To do so, living cells were immobilized on porous membranes and imaged in contact mode upon application of a low force (~100 pN) to preserve cell surface structure integrity. Representative deflection images of the *E. coli* wild type (WT) and its mutant derivative genetically modified to express the O-antigen at their surface (*E. coli* LPS^+)[42] are provided in Fig. 1 together with the results pertaining to *L. lactis* WT and *L. lactis* mutants lacking their native surface polysaccharide pellicle (*L. lactis* PSP^-).[43] The *E. coli* WT cell surface

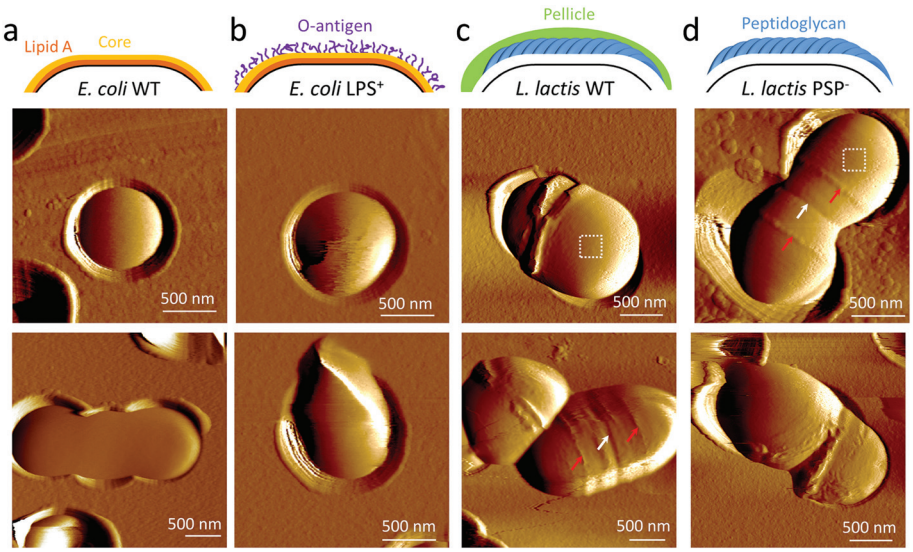

Fig. 1 Atomic force microscopy-based imaging of living bacteria mechanically trapped in porous membranes. Deflection images recorded in 10 mM KNO_3 solution for *E. coli* WT (a), *E. coli* modified to express the O-antigen (*E. coli* LPS$^+$; b), *L. lactis* WT (c) and *L. lactis* mutants devoid of surface polysaccharide pellicle (*L. lactis* PSP$^-$; d). White and red arrows in (c, d) indicate the division septum and ring-like structures, respectively. White boxes correspond to the areas where surface roughness was measured.

is smooth and featureless both at the cell pole (Fig. 1a top) and on the side wall (Fig. 1a bottom). In contrast, *E. coli* LPS$^+$ exhibit distinguishable features (Fig. 1b) possibly due to an alteration of the cell surface upon scanning, a finding that is consistent with the presence of a flexible O-antigen layer at the bacterial surface. As far as *L. lactis* cells are concerned, no major differences in cell surface features could be seen on the images for the WT and for the modified *L. lactis* PSP$^-$ strains. However, roughness analysis revealed that the WT strain is slightly smoother (R_q = 0.7 ± 0.2 nm measured on n = 15 areas of 200 nm × 200 nm) than the PSP$^-$ mutant (R_q = 1.4 ± 0.4 nm measured on n = 8 areas of 200 nm × 200 nm), most likely due to the disappearance of the polysaccharidic outer layer and exposure of the peptidoglycan (PG) layer on the PSP$^-$ strain, in line with previously reported observations.[43,44] Both cell types are marked by a well-defined division septum (Fig. 1c and d, white arrows) and characteristic ring-like structures located at a certain distance from the septum (Fig. 1c and d, red arrows). In agreement with previous suggestions from the literature,[44,45] these structures possibly define the position of the division site and are reminiscent of other Gram-positive bacteria such as streptococci or staphylococci.[45,46]

Electrokinetics of bacteria and G8.5 PAMAM-COOH dendrimers

In this section, we address the impact of solution pH on the electrostatic features of the here-adopted bacterial interphases and those of G8.5 PAMAM-COOH dendrimer nanoparticles. Fig. 2a and b display the dependence of the electrophoretic mobility μ of the four bacterial strains of interest on the concentration of KNO_3 electrolyte at pH 6.0 (Fig. 2a) and pH 3.5 (Fig. 2b). At pH 6.0, μ is negative for all strains and it decreases (in absolute value) with increasing background electrolyte concentration as a result of significant cell charge screening. At pH 3.5, this dependence of μ on the salt concentration is basically maintained for all strains. In addition, a significant decrease in $|\mu|$ is observed at low salt concentrations for *L. lactis* PSP$^-$ with decreasing pH from 6 to 3.5, whereas μ for *E. coli* WT and *L. lactis* WT cells remains quasi-independent of the solution pH over the whole range of salinity conditions investigated. The striking feature is the nearly zero mobility of *E. coli* LPS$^+$ at pH 3.5. The results obtained at pH 6 and pH 3.5 *versus* the salt concentration for *E. coli* WT and *L. lactis* WT cells are qualitatively in line with the generic electrokinetic properties expected for bacteria[47,48] and the protolytic features of their major ionogenic surface sites. In detail, the negative charge in *L. lactis* WT originates from the phosphate groups contained in the phosphodiester bonds that link the hexasaccharide repeating units of the pellicle.[43] In the absence of the pellicle, the charges most likely stem from the D-Asp residues of the PG interpeptide crossbridge[49] or the presence of residual lipoteichoic acids (LTA) at the cell surface.[50,51] The results obtained for *E. coli* LPS$^+$ highlight the peculiar physicochemical cell surface properties conferred by the O-antigen LPS component that is absent in the *E. coli* WT strain. LPS include three components: the lipid A, the core oligosaccharide and the O-antigen, the latter forming the outermost layer of the cell envelope (schematic of Fig. 1b). The O-antigen mostly comprises repeats of 3- to 8-sugar units.[52] The *E. coli* LPS$^+$ strain used in this work (MG1655 *wbbL* restored) is composed of 5-sugar unit repeats.[52] The negative charge carried by *E. coli* stems from the ester-linked phosphate groups within the lipid A region, as well as the carbonyl groups of KDO and phosphate groups of phosphorylated sugars of the core.[53,54]

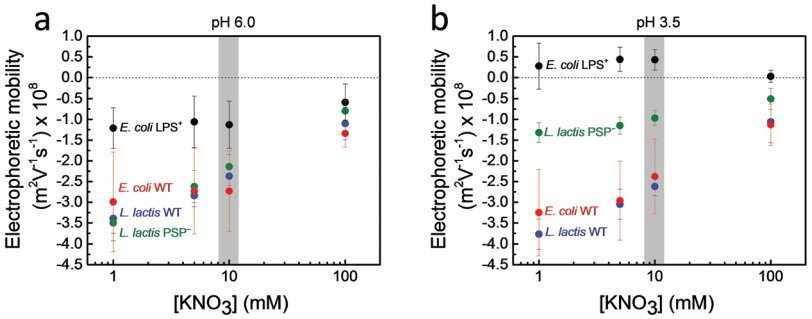

Fig. 2 Electrokinetic properties of the bacterial strains. Electrophoretic mobility of *E. coli* WT (red symbols), *E. coli* LPS$^+$ (black symbols), *L. lactis* WT (blue symbols) and *L. lactis* PSP$^-$ (green symbols) as a function of KNO_3 concentration at pH 6.0 (a) and pH 3.5 (b). The shaded areas indicate the electrolyte concentration at which AFM measurements were performed.

The O-antigen consists of hydrophilic sugar residues which tend to be uncharged, therefore acting as a barrier that shields the apparent negative charge carried by the bacteria.[55–58] In the current study, the shielding effect is particularly pronounced at pH 3.5, where the presence of the O-antigen totally cancels out the negative charge within the lipid A and the core layer of *E. coli*. Altogether, the electrokinetic signatures depicted in Fig. 2 highlight the significant modulation of the overall defining electrostatic properties of bacterial cell surfaces according to both their cell envelope structure (Gram-negative *E. coli vs.* Gram-positive *L. lactis*) and the nature of their polysaccharidic decoration (O-antigen *vs.* pellicle).

Additionally we measured the electrokinetic properties of carboxylate-terminated polyamidoamine dendrimer NPs (PAMAM-COOH, generation 8.5) under the pH and salinity conditions adopted in Fig. 2 (Fig. 3). PAMAM-COOH dendrimers are soft (*i.e.* ion/water permeable) NPs consisting of a hyperbranched amino-core with protonable tertiary amine groups and of a peripheral surface layer, the locus of dissociable carboxylic groups (Fig. 4). Fig. 3 highlights the salt-mediated screening of the effective charge carried by dendrimer NPs, especially at pH 3.5, and it further evidences a

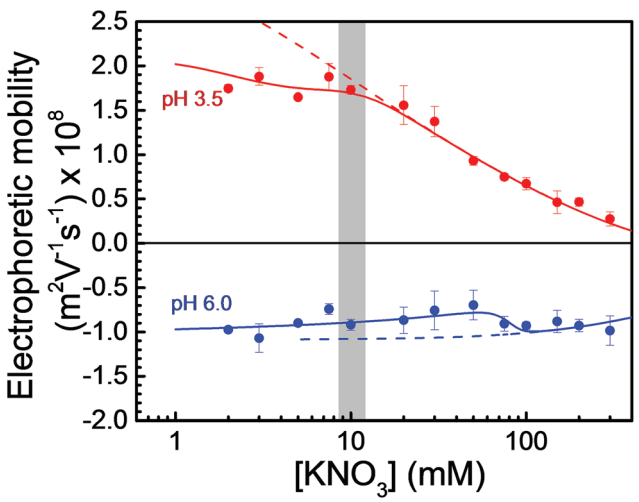

Fig. 3 Electrokinetic properties of dendrimer nanoparticles. Electrophoretic mobility of G8.5 PAMAM-COOH dendrimers as a function of KNO_3 electrolyte concentration at pH 6.0 (blue symbols) and 3.5 (red symbols). Experimental data are represented by points, whereas dotted and solid lines correspond to theoretical modeling extensively detailed in ref. 26. Adapted from ref. 26 with permission from The Royal Society of Chemistry.

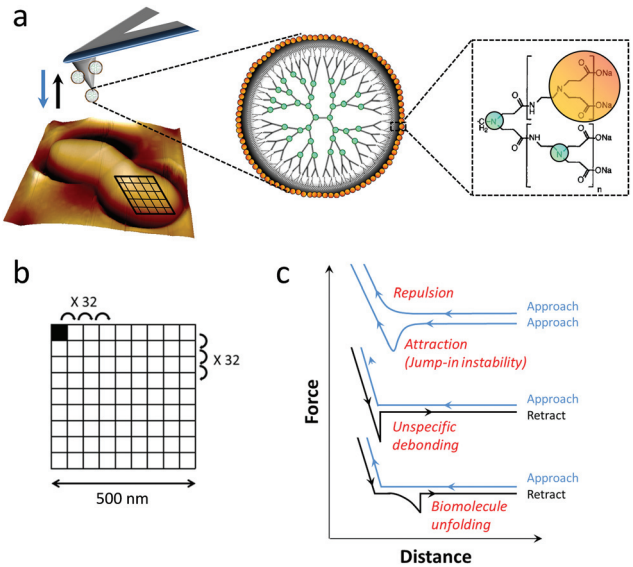

Fig. 4 Schematics of single-NP force spectroscopy measurements. (a) Carboxylate-terminated poly(amidoamine) (PAMAM) dendrimers of generation 8.5 – consisting of secondary and protonable tertiary amine groups located at the branching points of the particle core (green circles) and dissociable carboxylic groups that terminate each branch of the structure (orange circles) – are grafted on AFM tips using amino-carboxylate linking chemistry. Force measurements are recorded under liquid conditions at the surface of a living bacterium. For this purpose, a virtual mesh of 32 × 32 pixels (b) is defined at the microbial surface. At each pixel, the tip is approached to (blue arrow in a) and retracted from (black arrow in a) the biosurface, resulting in a force distance curve composed of an approach (blue curves in c) and a retraction regime (black curves in c). Approach of the tip from the surface can result either in repulsion or attraction (c, top blue curves). After the contact is established, the tip may de-bond from the sample in an unspecific manner (c, black middle curve) or may lead to surface biomolecule unfolding (c, black bottom curves).

change in the sign of the electrophoretic mobility μ of G8.5 PAMAM-COOH dendrimers with increasing pH from 3.5 to 6.0. As extensively detailed in a preceding report, PAMAM-COOH electrokinetics is dominated at pH 3.5 by intraparticulate protonated tertiary amine groups which leads to positive μ regardless of the salt concentration.[26] In contrast, the carboxylic groups located in the peripheral dendrimer shell are nearly completely dissociated at pH 6.0, which leads to negative NP mobility under such pH conditions. The reader is referred to the previous publication by the authors for further details on the peculiar pH- and monovalent electrolyte concentration-dependent electrohydrodynamic features of such G8.5 PAMAM dendrimers that display interfacial zwitterionic functionality.[26]

AFM force spectroscopy measurements

In light of the above ensemble-averaged electrokinetic properties identified for dispersions of PAMAM-COOH dendrimer NPs, for *E. coli* and *L. lactis* bacteria, it is anticipated that the adhesion of dendrimer NPs onto the microorganisms is governed – at least partially – by electrostatic interactions that should differ from one bacterium to another depending on their cell envelope composition and structure. To test this hypothesis at the relevant nanometric scale, the adhesion forces between G8.5 PAMAM dendrimers and the surface of the (living) bacteria of interest were measured using AFM-based force spectroscopy. To do so, PAMAM NPs were covalently grafted on the AFM tips *via* the amino-carboxy linking chemistry detailed in the Methods section, resulting in the attachment of a single NP at the apex of the tip (Fig. 4a).[26] Working in so-called force-volume mode,[59,60] a virtual mesh of 32 × 32 pixels (which corresponds to 500 nm × 500 nm surface area) was created at the cell surface (illustrated in Fig. 4b), where approach and retract curves were then recorded in each pixel. This allows the establishment of a spatial mapping of the interaction force between the dendrimer NPs and bacterial surfaces. In detail, the approach regime (Fig. 4c, blue curves) allows sensing long range electrostatic interactions between the two entities before contact is established, revealing either repulsion or attraction of the tip from/to the surface. After contact, inspection of the retraction regime (Fig. 4c, black curves) enables the identification of whether or not the NP bound to the bacterial cell-wall, and the evaluation of the adhesion force required to detach the NP from the biosurface and the (possible) unfolding of the biomolecules engaged in the interaction (Fig. 4c, bottom black curve). The obtained adhesion maps, adhesion-force histograms (derived from the retraction force measurements, Fig. 4c) and the representative force–distance curves as measured in 10 mM KNO_3 electrolyte concentration at pH 6 between G8.5 dendrimer PAMAM-COOH NPs and the 4 bacterial strains of interest in this study are reported in Fig. 5. For all bacterial strains examined, it can be seen on most of the approach curves (Fig. 5, blue curves) that the force gradually increases as the distance between the dendrimer-coated tip and the cell surface decreases, reflecting a repulsive NP–bacterium interaction profile (Fig. 4c, top blue curves). The percentage of non-adhesive events detected upon retraction of the NP-decorated tip from the cell surface is very high (>98%; Fig. 5, black curves). At pH 6 and 10 mM KNO_3 concentration, the effective surface charge carried by the NPs is systematically negative (Fig. 3, shaded area) and so is the charge of the bacterial cell surfaces (Fig. 2a). The repulsion evidenced by AFM-single NP force measurements supports that electrostatic interactions prevent the attachment of the NPs at the microbial surfaces under such pH condition.

We also determine adhesion maps, adhesion force-histograms and representative force–distance curves obtained when dendrimers interact with the bacterial cells at pH 3.5 in 10 mM electrolyte concentration (Fig. 6). Contrary to the situation previously detailed, measurements now reveal a high frequency of dendrimer NP–*L. lactis* WT adhesion events on the retraction curves (53 to 55%) with adhesion forces ranging from 100 pN to 500 pN (Fig. 6a). Two types of force–distance curves profiles may be distinguished: (i) profiles with a marked single adhesion peak observed upon retraction of the NP-decorated tip in continuity of the linear compliance region (with therefore no sign of surface biocompound extension, Fig. 4c, middle black curve and Fig. 6a, top black curve), and (ii) profiles with adhesion peaks detected at bacteria to NP separation distances reminiscent of protein/polysaccharide unfolding (Fig. 4c, bottom black curve and Fig. 6a, bottom black curve). These findings suggest that the interactions between positively-charged NPs and the negatively charged surface of *L. lactis* WT (Fig. 2 and 3) are primarily mediated by attractive electrostatic interactions, in line with the sign of the force measured in the approach phase, and that they involve the binding and subsequent unfolding of biomolecules to/at the cell surface. Some multiple adhesive events were sometimes observed in some of the performed AFM force experiments. We cannot exclude that in the presence of a fuzzy polysaccharidic layer, few NPs – and not only the one located at the tip apex – could be involved in the interaction. A closer inspection of the adhesion force-maps further reveals that NP–cell binding sites are non-homogenously distributed over the cell surface and form clusters or patches. This may indicate that (i) the polysaccharidic pellicle does not form a monolayer at the surface of *L. lactis*, (ii) the pellicle is heterogeneous in composition and NPs bind differently to the different pellicle-constituting polysaccharides, and/or that (iii) NPs bind to surface biomolecules other than those stemming from the bacterial pellicle. At this stage, it is worth mentioning that AFM imaging revealed a homogeneous pellicle layer (Fig. 1c) reported to form a compact and continuous cell surface structure composed of polysaccharides made of hexasaccharide repeating units (containing two glucoses (Glc), two *N*-acetylglucosamine (GlcNAc), one rhamnose (Rha), and one D-galactose (Galf)) residues linked *via* phosphodiester bonds.[43] With these latter elements in mind, it is most likely that the density of the *L. lactis* surface pellicle does not allow binding of the NP to compounds underneath the layer, and that the observed adhesive patches are due to NP anchoring sites heterogeneously distributed within the polysaccharidic layer. In other terms, this means that either the secreted polysac-

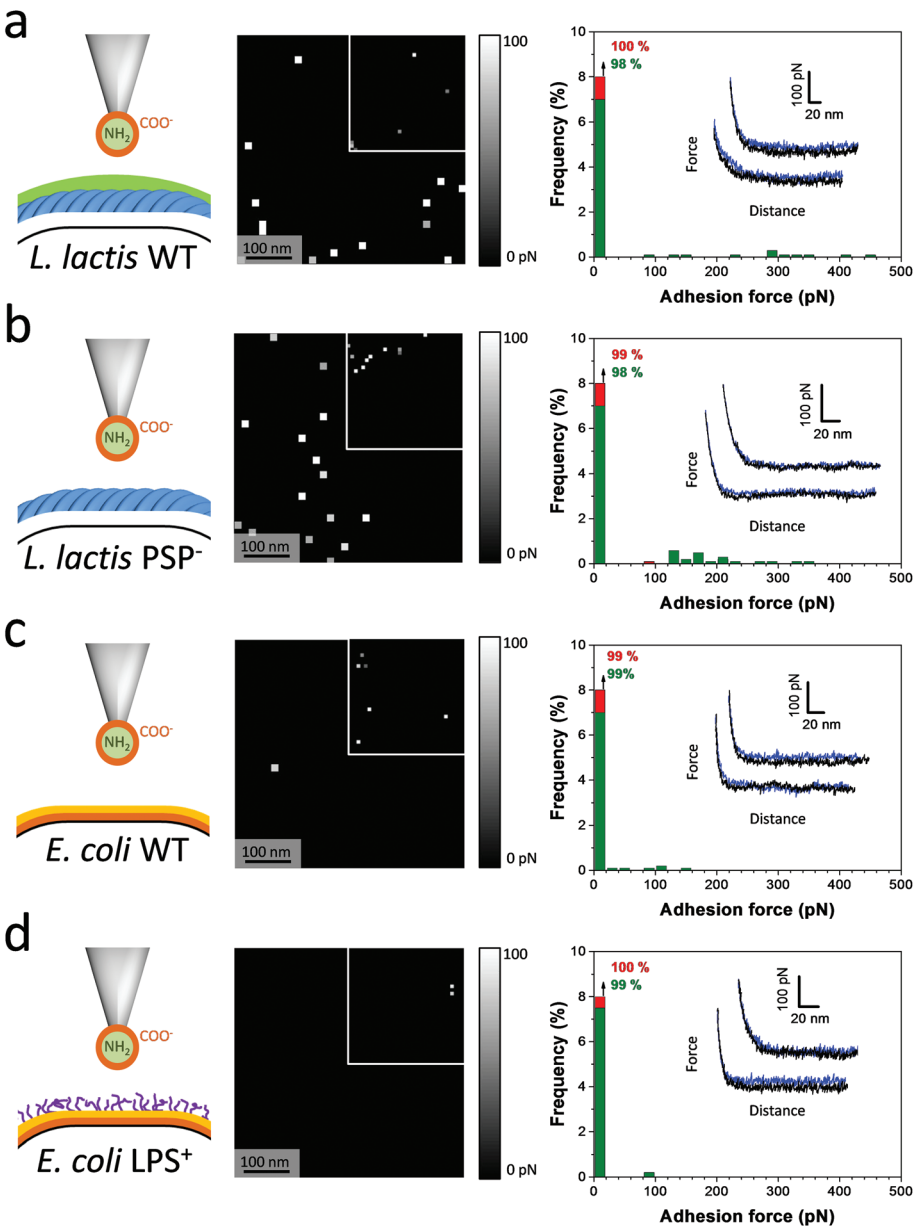

Fig. 5 Single-NP force spectroscopy reveals no adhesion between PAMAM-COOH nanoparticles and bacteria at pH 6.0. Adhesion force maps (500 nm × 500 nm) and adhesion force histograms with representative force–distance curves (blue: approach curves; black: retract curves) obtained by recording spatially resolved force curves using dendrimer-decorated tips at the surface of *L. lactis* WT (a), *L. lactis* PSP$^-$ (b), *E. coli* WT (c) and *E. coli* LPS$^+$ (d) (n = 1024 curves for each cell). Grey scales on the maps correspond to the 0–100 pN range, black pixels correspond to the absence of an adhesion event. The insets on the maps show maps from independent experiments. The green and red colors in the histograms at the right side correspond to two independent experiments.

charides are localized as patches and are thus totally absent at some cell surface spots, or that there are present all over the cell but in various proportions. A high level of adhesive events was also detected at the surface of *L. lactis* PSP$^-$ (38 and 68%, Fig. 6b). In the absence of the peripheral pellicle, the NP probably binds to the bacterial surface *via* electrostatic interactions between the positively-charged dendrimer and the surface biocompounds that carry a negative charge conferred either by the interpeptide crossbridges of PG or the presence of LTA. It is also possible that the NPs bind to the recently-discovered rhamnan polysaccharide trapped inside the PG and exposed to the surrounding medium at the cell surface in the absence of PSP.[61] The distribution patterns of the binding events vary from one map to another (Fig. 6b), and so does the shape of the retraction force–distance curves (some curves reveal biomolecules unfolding and others do not). This suggests that the NPs can interact either with the homogeneous rigid surface compounds forming the PG or with some residual LTA or

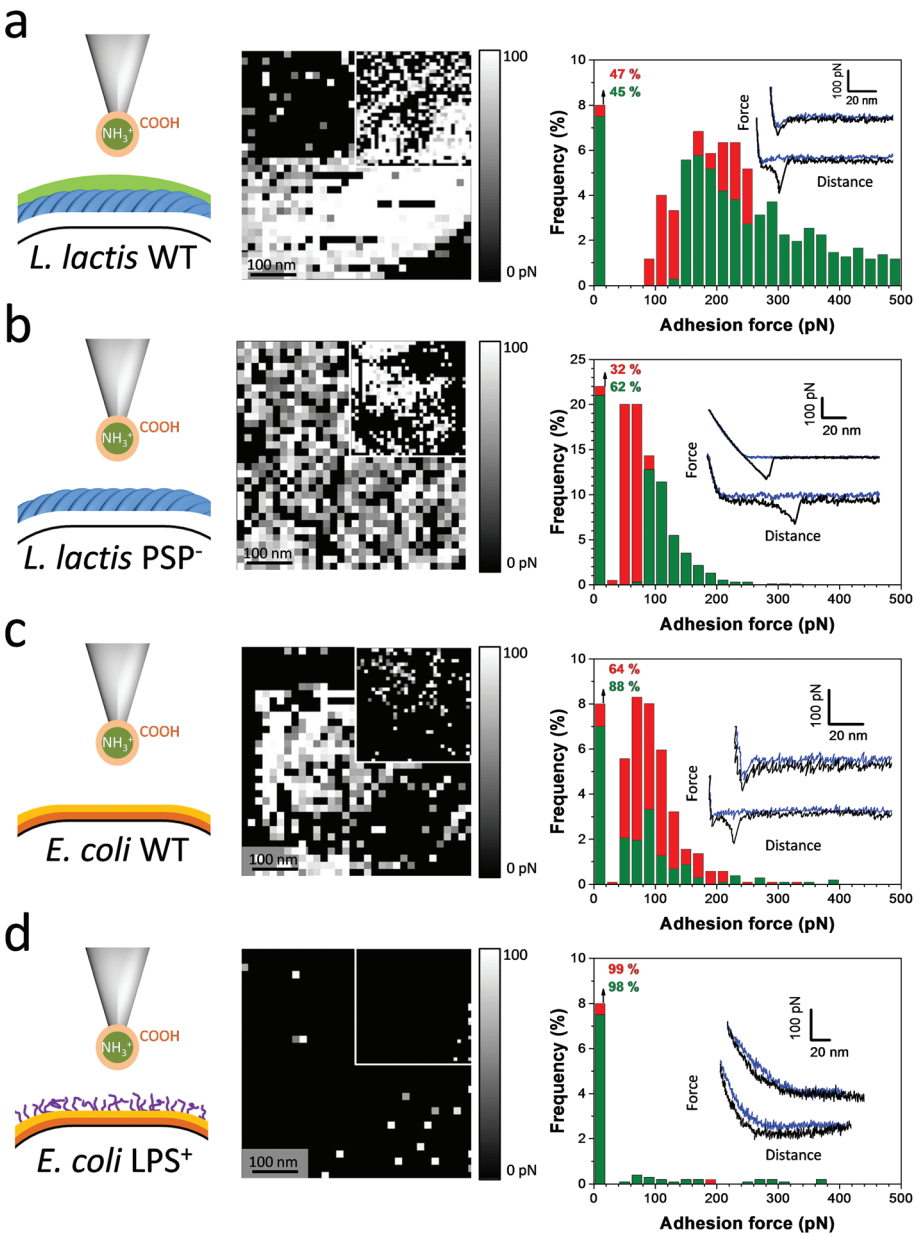

Fig. 6 NP–bacteria interaction features at pH 3.5. Adhesion force maps (500 nm × 500 nm) and adhesion force histograms with representative force–distance curves (blue: approach curves; black: retraction curves) obtained by recording spatially resolved force curves using dendrimer-decorated tips at the surface of *L. lactis* WT (a), *L. lactis* PSP$^-$ (b), *E. coli* WT (c) and *E. coli* LPS$^+$ (d) (n = 1024 curves for each cell). Grey scales on the maps correspond to the 0–100 pN range, black pixels correspond to the absence of the adhesion event. The insets on the maps show maps from independent experiments. The green and red colors in the histograms at the right side correspond to two independent experiments.

rhamnan polysaccharides at the cell surface.[61] The magnitude of the adhesion forces (ranging from 50 to 200 pN for *L. lactis* PSP$^-$ as compared to 100 to 500 pN for *L. lactis* WT) qualitatively correlates with the values of $|\mu|$ measured at pH 3.5 for these two strains (0.92 and 2.62 × 10^{-8} m^2 V^{-1} s^{-1} for *L. lactis* PSP$^-$ and *L. lactis* WT, respectively). This ensemble of results strongly suggests that the pellicle surface structure does not govern on its own but rather mediates the interaction between the positively-charged NPs and the cell wall as a whole, most probably by increasing the effective negative charge carried by the bacterial envelope and 'experienced' by the NPs when in the vicinity of – or in contact with – the cell surface.

The adhesion features of dendrimer NPs on the surface of *E. coli* WT are shown in Fig. 6c at pH 3.5 and 10 mM electrolyte concentration. The frequency of detected adhesion events ranges from 12 to 36% with adhesion forces in the 50 pN–250 pN range. Whereas the electrophoretic mobility of *E. coli* WT is basically similar to that of *L. lactis* WT under the here-examined pH conditions, the adhesion of dendrimer NPs onto the former cell surface type is significantly lower. This result

demonstrates that the magnitude of the interactions between charged NPs and Gram-positive or Gram-negative microorganisms cannot generally be derived on the sole basis of their respective surface charges obtained from electrokinetic measurements. Instead, the analysis should necessarily integrate the contributions from the respective components of the cell envelope, that is the oligosaccharidic core and lipid A anchored in the outer lipid membrane of the Gram-negative *E. coli*, and the exposed peptidoglycan covered by the pellicle of the Gram-positive *L. lactis*. In contrast to *E. coli* WT cells, repulsive force–distance profiles are measured at pH 3.5 when the NP-functionalized tip approaches the surface of *E. coli* LPS$^+$ (Fig. 6d, blue curves), and no NP–*E. coli* LPS$^+$ adhesion events could be detected in the retraction stage (Fig. 6d, black curves). These findings are qualitatively consistent with the quasi-neutral charge carried by *E. coli* LPS$^+$ at pH 3.5 (Fig. 2) and the positive (effective) charge carried by dendrimers under such pH conditions. In agreement with the literature,[53,55,56,58] this result confirms that expression of the O-antigen part of the LPS leads to a complete neutralization of the negative charge carried by the supporting cell envelope of *E. coli* and it emphasizes the importance of surface polysaccharides in mediating NP/microorganism interactions. In addition, the presence of the flexible O-antigen LPS layer likely leads to a significant repulsive contribution (of steric origin) to the overall NP–*E. coli* LPS$^+$ interaction, thereby preventing adhesion of NPs onto the cell envelope, regardless of the pH-dependent effective charge it carries (which translates into the quasi total absence of adhesion events on the map Fig. 6d).

Conclusions

Cell surface polysaccharides have been suggested as important actors in the attachment/adhesion of NPs onto bacteria. In this study, electrokinetics and single-NP force spectroscopy are employed to address the interaction forces acting between PAMAM-COOH G8.5 dendrimer NPs and the surface of Gram-positive *L. lactis* and Gram-negative *E. coli* cells expressing or not polysaccharides at their surface. Analysis of measurements obtained under pH conditions corresponding to distinct electrostatic features of the bacterial envelopes and/or of the NPs makes it possible to decipher the relative contribution of electrostatic interaction forces in the binding of the NPs to the four bacterial strains of interest. We clearly evidence that regardless of the pH conditions NP adhesion onto the cell surface is suppressed in the presence of the O-antigen glycopolymeric layer whereas the occurrence or not of NP–cell adhesion events closely meets expectations based on the electrokinetic results. This work demonstrates that a refined assessment of the interactions between NPs and biological surfaces highly benefits from the joint consideration of electrokinetic measurements, conducted at the NP dispersion and cell population scales, and of AFM-single NP measurements performed at the single cell level. These techniques represent a powerful platform for a rapid identification of the role played by cell surface biomolecules in mediating the NP approach towards complex and diverse cell wall structures or in governing NP bioadhesion.

Methods

Bacterial strains

Two types of bacteria are used in this study: the Gram-positive bacterium *Lactococcus lactis* (strain MG1363) and the Gram-negative bacterium *Escherichia coli* (K12, strain MG1655). The cell envelope of Gram-negative bacteria features a thin layer of peptidoglycan (PG) overlaid by an outer membrane, in which are anchored LPS covering 75% of the cell surface.[62,63] In contrast, the Gram-positive cell envelope is made of a thick layer of PG crossed by teichoic acids, sometimes covered by an outer layer of polysaccharides.[64–66] The current work deals with four bacterial strains: *E. coli* wild type (WT) K-12 M1655 (*E. coli* genetic stock center #CGSC6300) that naturally do not produce the O-antigen due to the interruption of the *wbbL* gene by an insertion element (IS), an *E. coli* mutant genetically modified to express the O-antigen at their surface by restoring the *wbbL* gene (denoted as *E. coli* LPS$^+$ in the manuscript),[42] *L. lactis* wild type (WT) MG1363, and an *L. lactis* mutant devoid of the native surface polysaccharide pellicle (PSP) – VES5748 (hereafter denoted as *L. lactis* PSP$^-$).[43] The repeat unit structures of the O-antigen of the restored LPS$^+$ strain correspond to the O-antigen O16 with a linear chain of β-D-galactose, α-D-glucose, α-L-rhamnose branched with an O acetyl and an α-D-*N* acetyl glucosamine branched with an α-D-glucose.[52]

L. *lactis* strains were grown for 12 h in M17 medium supplemented with 0.5% glucose, at 30 °C without shaking. *E. coli* strains were grown for 12 h in Lysogeny Broth (LB) at 37 °C with shaking at 200 rpm.

Carboxylated PAMAM dendrimers

Half-generation G8.5 carboxylate-terminated poly(amidoamine) (PAMAM) dendrimers dissolved in water were purchased from Dendritech (Dendritech Inc., U.S.A.). They consist of a hyperbranched amino-core which possesses protonable tertiary amine groups and a peripheral shell made of dissociable carboxylic groups.[5,13,67] Each dendrimer contains $2(2^{n+1} - 1)$ tertiary amine groups and 2^{n+2} carboxylic groups,[13] n being the dendrimer generation with $n = 9$ for the G8.5 dendrimer generation adopted in this work (*i.e.* 2046 tertiary amine and 2048 carboxylic groups).

Bacterial electrophoretic mobility measurements

The electrophoretic mobility measurements of the bacteria of interest in this work were performed at room temperature using a Zetaphoremeter IV (CAD Instrumentations, Les Essarts le Roi, France). For this purpose, cells were harvested and rinsed twice by centrifugation at 5000*g* for 2 min, and resuspended in KNO_3 (Sigma-Aldrich, purity >99%) to a final $OD_{600\ nm}$ of 0.4 (10^8 cells per mL). The cell suspensions were then diluted at an $OD_{600\ nm}$ of 0.04 in 1, 5, 10 and 100 mM

KNO_3 solutions and the solution pH was adjusted at the desired value (3.5 and 6 in this study) after proper addition of HNO_3 (0.1 M, Sigma, purum p.a.) and KOH (0.1 M, VWR, convol Normadose) solutions. The determination of the mobility consisted in following the displacements of bacteria in a quartz Suprasil® rectangular capillary under conditions where a constant direct-current electric field (around 800 V m^{-1}) is applied. Migration of bacteria was measured by tracking the reflection by the bioparticles of a laser beam at a 90° angle with the use of a charge-coupled device camera. Trajectories were recorded in real time and processed with the help of image analysis software, thus making possible evaluation of cells' electrophoretic mobilities. For each electrolyte concentration tested, measurements were performed in triplicate. Under all conditions adopted in this work, we found a monomodal Gaussian distribution of electrophoretic mobilities as a function of the number of tracked cell trajectories.

Nanoparticles' electrophoretic mobility measurements

The electrophoretic mobility of G8.5 PAMAM-COOH dendrimers was measured as a function of KNO_3 (Sigma-Aldrich, purity >99%) concentration at room temperature using a Zetasizer Nano ZS instrument (Malvern Instruments). Desired pH values were adjusted by proper addition of HNO_3 (0.1 M, Sigma, purum p.a.) and KOH (0.1 M, VWR, convol Normadose) solutions. Each reported data point is the average of at least 3 distinct mobility acquisitions. The particle radius (of ~4.5 nm) was also measured (data not shown) with no sign of aggregation under the pH and salt concentration conditions relevant in this work.

Atomic force microscopy

AFM measurements were performed on an Icon Dimension from Bruker Corporation (Santa Barbara, CA) equipped with a home-made liquid cell in 10 mM KNO_3 electrolyte solution at room temperature. Contact mode imaging was adopted using oxide sharpened microfabricated Si_3N_4 cantilevers with a nominal spring constant of ~0.01 N m^{-1} (MSCT, Bruker Corporation). Bacteria were immobilized by mechanical trapping into porous polycarbonate membranes (Millipore, Billerica, MA) with a pore size similar to the cell dimension.[68] After filtering a cell culture, the filter was gently rinsed with the buffer, carefully cut (~1 cm × 1 cm), attached to a steel sample puck using a small piece of double sided adhesive tape and mounted into the AFM liquid cell without dewetting. Based on the previous work on the size and morphology of *E. coli* and *Lactobacillus plantarum* observed by AFM,[69,70] it appears that bacillus rod-shape bacteria trapped in such porous membranes expose their polar sides in single pores whereas their lateral side structures can only fit within pore doublets or triplets.

Regarding force spectroscopy measurements, bacteria were first localized using a bare tip, and the latter was subsequently replaced by a NP-functionalized tip. NP-decorated AFM tips were generated upon covalent attachment of PAMAM-COOH dendrimers to the AFM tips. For this purpose, MSCT cantilevers were used and their spring constants (of nominal values 0.03 N m^{-1}) were accurately determined on the basis of the thermal noise method. In detail, tips were first functionalized with amine groups. To do so, they were washed for 10 min with Piranha solution (3 : 1 mixture of concentrated H_2SO_4 and 30% H_2O_2 solution), rinsed thoroughly with ultrapure water, dried with N_2, and finally rinsed 3 times with chloroform and twice with ethanol, dried and placed in a UV-ozone cleaner for 15 min. Cleaned cantilevers were immersed overnight in an ethanolamine solution (3.3 g of ethanolamine in 6 mL of DMSO), then washed three times with DMSO and twice with ethanol, and finally dried with N_2. The dendrimers were then covalently attached to the tip *via N*-hydroxysuccinimide (NHS) 1-ethyl-3-(3-dimethylaminopropyl)-carbodiimide (EDC) surface chemistry. Dendrimers were immersed in NHS-EDC solution at a concentration allowing 10 out of the 2048 carboxylic surface groups of a dendrimer particle to be activated. To achieve such an activation level, 50 μL of the dendrimer solution received from the provider (1.06×10^{-4} mol L^{-1}) were diluted in 2 mL ultrapure water containing EDC at 5 mg L^{-1} and NHS at 5.6 mg L^{-1}. The amine-decorated tips were then immediately immersed in the activated-dendrimer solution, allowed to rest for 1 hour, rinsed in ultrapure water and stored in water until use.

Adhesion maps were obtained by recording 32 × 32 force–distance curves on 500 nm × 500 nm areas of the bacterial surface. All force curves were recorded in 10 mM KNO_3 solution with a maximum applied force of 250 pN, using a constant approach and retraction speed of 1 μm s^{-1}.

Conflicts of interest

There are no conflicts to declare.

Acknowledgements

This work was supported by the French National Programme Ec2CO-Ecodyn/MicrobiEN (TOXSCALE project) and by the CNRS National Program PEPS-FaiDoRA (NanodUP project). CB and JMG are supported by the French Government's Investissements d'Avenir Program, Laboratoire d'Excellence "Integrative Biology of Emerging Infectious Diseases" (grant no. ANR-10-LABX-62-IBEID) and the Fondation pour la Recherche Médicale grant (Equipe FRM DEQ20140329508).

References

1 S. Svenson, *Eur. J. Pharm. Biopharm.*, 2009, **71**, 445–462.
2 K. Jain, P. Kesharwani, U. Gupta and N. K. Jain, *Int. J. Pharm.*, 2010, **394**, 122–142.
3 A. E. Nel, L. Madler, D. Velegol, T. Xia, E. M. V. Hoek, P. Somasundaran, F. Klaessig, V. Castranova and M. Thompson, *Nat. Mater.*, 2009, **8**, 543–557.

4 D. A. Tomalia, H. Baker, J. Dewald, M. Hall, G. Kallos, S. Martin, J. Roeck, J. Ryder and P. Smith, *Polym. J.*, 1985, **17**, 117–132.
5 D. A. Tomalia and J. M. J. Frechet, *J. Polym. Sci., Part A: Polym. Chem.*, 2002, **40**, 2719–2728.
6 A. M. Caminade, A. Ouali, R. Laurent, C. O. Turrin and J. P. Majoral, *Coord. Chem. Rev.*, 2016, **308**, 478–497.
7 W. W. Gao, S. Thamphiwatana, P. Angsantikul and L. F. Zhang, *Wiley Interdiscip. Rev.: Nanomed. Nanobiotechnol.*, 2014, **6**, 532–547.
8 B. Noriega-Luna, L. A. Godinez, F. J. Rodriguez, A. Rodriguez, G. Z. L. de Larrea, C. F. Sosa-Ferreyra, R. F. Mercado-Curiel, J. Manriquez and E. Bustos, *J. Nanomater.*, 2014, 507273.
9 M. Selin, L. Peltonen, J. Hirvonen and L. M. Bimbo, *J. Drug Delivery Sci.*, 2016, **34**, 10–20.
10 X. Ming, L. Wu, K. Carver, A. Yuan and Y. Z. Min, *Nanoscale*, 2015, **7**, 12302–12306.
11 C. C. Fleischer and C. K. Payne, *Acc. Chem. Res.*, 2014, **47**, 2651–2659.
12 M. P. Monopoli, C. Aberg, A. Salvati and K. A. Dawson, *Nat. Nanotechnol.*, 2012, **7**, 779–786.
13 M. Moussa, C. Caillet, R. M. Town and J. F. L. Duval, *Langmuir*, 2015, **31**, 5656–5666.
14 N. J. Braun, M. C. DeBrosse, S. M. Hussain and K. K. Comfort, *Mat. Sci. Eng., C*, 2016, **64**, 34–42.
15 P. Foroozandeh and A. A. Aziz, *Nanoscale Res. Lett.*, 2015, **10**, 221.
16 M. Lundqvist, J. Stigler, T. Cedervall, T. Berggard, M. B. Flanagan, I. Lynch, G. Elia and K. Dawson, *ACS Nano*, 2011, **5**, 7503–7509.
17 P. Kesharwani, K. Jain and N. K. Jain, *Prog. Polym. Sci.*, 2014, **39**, 268–307.
18 F. Ruggeri, A. Akesson, P. Y. Chapuis, C. A. S. Nielsen, M. P. Monopoli, K. A. Dawson, T. G. Pomorski and M. Cardenas, *Soft Matter*, 2013, **9**, 8862–8870.
19 S. H. Lee, S. H. Choi, S. H. Kim and T. G. Park, *J. Controlled Release*, 2008, **125**, 25–32.
20 M. Labieniec and T. Gabryelak, *Mitochondrion*, 2008, **8**, 305–312.
21 J. H. Lee, K. E. Cha, M. S. Kim, H. W. Hong, D. J. Chung, G. Ryu and H. Myung, *Toxicol. Lett.*, 2009, **190**, 202–207.
22 X. J. Cai, R. R. Jin, J. L. Wang, D. Yue, Q. Jiang, Y. Wu and Z. W. Gu, *ACS Appl. Mater. Interfaces*, 2016, **8**, 5821–5832.
23 M. Ionov, A. Ihnatsyeu-Kachan, S. Michlewska, N. Shcharbina, D. Shcharbin, J. P. Majoral and M. Bryszewska, *Int. J. Pharm.*, 2016, **499**, 247–254.
24 N. Malik, R. Wiwattanapatapee, R. Klopsch, K. Lorenz, H. Frey, J. W. Weener, E. W. Meijer, W. Paulus and R. Duncan, *J. Controlled Release*, 2000, **68**, 299–302.
25 R. Jevprasesphant, J. Penny, R. Jalal, D. Attwood, N. B. McKeown and A. D'Emanuele, *Int. J. Pharm.*, 2003, **252**, 263–266.
26 A. Beaussart, C. Caillet, I. Bihannic, R. Zimmermann and J. F. L. Duval, *Nanoscale*, 2018, **10**, 3181–3190.
27 E. Alpaslan, B. M. Geilich, H. Yazici and T. J. Webster, *Sci. Rep.*, 2017, **7**, 45859.
28 C. Z. S. Chen and S. L. Cooper, *Biomaterials*, 2002, **23**, 3359–3368.
29 Z. V. Feng, I. L. Gunsolus, T. A. Qiu, K. R. Hurley, L. H. Nyberg, H. Frew, K. P. Johnson, A. M. Vartanian, L. M. Jacob, S. E. Lohse, M. D. Torelli, R. J. Hamers, C. J. Murphy and C. L. Haynes, *Chem. Sci.*, 2015, **6**, 5186–5196.
30 K. A. Heys, M. J. Riding, R. J. Strong, R. F. Shore, M. G. Pereira, K. C. Jones, K. T. Semple and F. L. Martin, *Analyst*, 2014, **139**, 896–905.
31 H. D. Lu, S. S. Yang, B. K. Wilson, S. A. McManus, C. Chen and R. K. Prud'homme, *Appl. Nanosci.*, 2017, **7**, 83–93.
32 N. S. Abadeer, G. Fulop, S. Chen, M. Kall and C. J. Murphy, *ACS Appl. Mater. Interfaces*, 2015, **7**, 24915–24925.
33 K. H. Jacobson, I. L. Gunsolus, T. R. Kuech, J. M. Troiano, E. S. Melby, S. E. Lohse, D. Hu, W. B. Chrisler, C. J. Murphy, G. Orr, F. M. Geiger, C. L. Haynes and J. A. Pedersen, *Environ. Sci. Technol.*, 2015, **49**, 10642–10650.
34 W. Jiang, K. Yang, R. W. Vachet and B. S. Xing, *Langmuir*, 2010, **26**, 18071–18077.
35 C. Yang, H. Xie, Q. C. Li, E. J. Sun and B. L. Su, *J. Colloid Interface Sci.*, 2015, **450**, 388–395.
36 M. A. Ansari, H. M. Khan, A. A. Khan, S. S. Cameotra, Q. Saquib and J. Musarrat, *J. Appl. Microbiol.*, 2014, **116**, 772–783.
37 P. T. Wong, S. Z. Tang, K. Tang, A. Coulter, J. Mukherjee, K. Gam, J. R. Baker and S. K. Choi, *J. Mater. Chem. B*, 2015, **3**, 1149–1156.
38 G. Francius, P. Polyakov, J. Merlin, Y. Abe, J. M. Ghigo, C. Merlin, C. Beloin and J. F. L. Duval, *PLoS One*, 2011, **6**, e20066.
39 A. Beaussart, M. Abellan-Flos, S. El-Kirat-Chatel, S. P. Vincent and Y. F. Dufrene, *Nano Lett.*, 2016, **16**, 1299–1307.
40 M. Mills, B. G. Orr, M. M. B. Holl and I. Andricioaei, *J. Phys. Chem. B*, 2013, **117**, 973–981.
41 A. N. Leistra, J. H. Han, S. Z. Tang, B. G. Orr, M. M. B. Holl, S. K. Choi and K. Sinniah, *J. Phys. Chem. B*, 2015, **119**, 5785–5792.
42 O. Rendueles, C. Beloin, P. Latour-Lambert and J. M. Ghigo, *ISME J.*, 2014, **8**, 1275–1288.
43 M. P. Chapot-Chartier, E. Vinogradov, I. Sadovskaya, G. Andre, M. Y. Mistou, P. Trieu-Cuot, S. Furlan, E. Bidnenko, P. Courtin, C. Pechoux, P. Hols, Y. F. Dufrene and S. Kulakauskas, *J. Biol. Chem.*, 2010, **285**, 10464–10471.
44 G. Andre, S. Kulakauskas, M. P. Chapot-Chartier, B. Navet, M. Deghorain, E. Bernard, P. Hols and Y. F. Dufrene, *Nat. Commun.*, 2010, **1**, 27.
45 C. Morlot, A. Zapun, O. Dideberg and T. Vernet, *Mol. Microbiol.*, 2003, **50**, 845–855.

46 A. Touhami, M. H. Jericho and T. J. Beveridge, *J. Bacteriol.*, 2004, **186**, 3286–3295.
47 J. F. L. Duval and F. Gaboriaud, *Curr. Opin. Colloid Interface Sci.*, 2010, **15**, 184–195.
48 F. Gaboriaud, E. Dague, S. Bailet, F. Jorand, J. Duval and F. Thomas, *Colloids Surf., B*, 2006, **52**, 108–116.
49 P. Veiga, M. Erkelenz, E. Bernard, P. Courtin, S. Kulakauskas and M. P. Chapot-Chartier, *J. Bacteriol.*, 2009, **191**, 3752–3757.
50 N. E. Kramer, H. E. Hasper, P. T. C. van den Bogaard, S. Morath, B. de Kruijff, T. Hartung, E. J. Smid, E. Breukink, J. Kok and O. P. Kuipers, *Microbiology*, 2008, **154**, 1755–1762.
51 L. Sijtsma, J. T. M. Wouters and K. J. Hellingwerf, *J. Bacteriol.*, 1990, **172**, 7126–7130.
52 Y. Q. Hong and P. R. Reeves, *J. Bacteriol.*, 2014, **196**, 1713–1722.
53 C. Capodici, S. Chen, Z. Sidorczyk, P. Elsbach and J. Weiss, *Infect. Immun.*, 1994, **62**, 259–265.
54 S. V. Zubova, A. Y. Ivanov and I. R. Prokhorenko, *Microbiology*, 2008, **77**, 293–297.
55 R. R. Boyer, S. S. Sumner, R. C. Williams, K. E. Kniel and J. M. McKinney, *Int. J. Food Microbiol.*, 2011, **147**, 228–232.
56 M. M. Domingues, P. M. Silva, H. G. Franquelim, F. A. Carvalho, M. Castanho and N. C. Santos, *Nanomedicine*, 2014, **10**, 543–551.
57 M. U. Hammer, A. Brauser, C. Olak, G. Brezesinski, T. Goldmann, T. Gutsmann and J. Andra, *Biochem. J.*, 2010, **427**, 477–488.
58 A. Kumar, D. Mallik, S. Pal, S. Mallick, S. Sarkar, A. Chanda and A. S. Ghosh, *FEMS Microbiol. Lett.*, 2015, **362**, fnv112.
59 V. Dupres, F. D. Menozzi, C. Locht, B. H. Clare, N. L. Abbott, S. Cuenot, C. Bompard, D. Raze and Y. F. Dufrene, *Nat. Methods*, 2005, **2**, 515–520.
60 S. El-Kirat-Chatel and A. Beaussart, in *Nanotechnology to Aid Chemical and Biological Defense*, ed. T. A. Camesano, 2015, pp. 1–15.
61 I. Sadovskaya, E. Vinogradov, P. Courtin, J. Armalyte, M. Meyrand, E. Giaouris, S. Palussiere, S. Furlan, C. Pechoux, S. Ainsworth, J. Mahony, D. van Sinderen, S. Kulakauskas, Y. Guerardel and M. P. Chapot-Chartier, *mBio*, 2017, **8**, e01303-17.
62 J. W. Costerton, J. M. Ingram and K. J. Cheng, *Bacteriol. Rev.*, 1974, **38**, 87–110.
63 A. P. Le Brun, L. A. Clifton, C. E. Halbert, B. H. Lin, M. Meron, P. J. Holden, J. H. Lakey and S. A. Holt, *Biomacromolecules*, 2013, **14**, 2014–2022.
64 M. P. Chapot-Chartier and S. Kulakauskas, *Microb. Cell Fact.*, 2014, **13**, S9.
65 J. Delcour, T. Ferain, M. Deghorain, E. Palumbo and P. Hols, *Anton. Leeuw. Int. J. G.*, 1999, **76**, 159–184.
66 C. Weidenmaier and A. Peschel, *Nat. Rev. Microbiol.*, 2008, **6**, 276–287.
67 Y. H. Niu, L. Sun and R. A. Crooks, *Macromolecules*, 2003, **36**, 5725–5731.
68 G. Andre, K. Leenhouts, P. Hols and Y. F. Dufrene, *J. Bacteriol.*, 2008, **190**, 7079–7086.
69 G. Andre, M. Deghorain, P. A. Bron, I. I. van Swam, M. Kleerebezem, P. Hols and Y. F. Dufrene, *ACS Chem. Biol.*, 2011, **6**, 366–376.
70 R. M. Present, E. Rotureau, P. Billard, C. Pagnout, B. Sohm, J. Flayac, R. Gley, J. P. Pinheiro and J. F. L. Duval, *Phys. Chem. Chem. Phys.*, 2017, **19**, 29114–29124.